Results in Physics 16 (2020) 102881

Contents lists available at ScienceDirect

Results in Physics

journal homepage: www.elsevier.com/locate/rinp

Resonant transmission through periodic subwavelength terahertz metallic slits based on a quartz plate

Sungjun Yoo[a,1], Jong-Eon Park[a,*], Hosung Choo[b,1]

[a] Metamaterial Electronic Device Research Centre, Hongik University, Seoul, Republic of Korea
[b] School of Electronic and Electrical Engineering, Hongik University, Seoul, Republic of Korea

ABSTRACT

This article proposes the resonant transmission characteristic through the periodic subwavelength metal-insulator-metal (MIM) waveguide on a quartz plate at terahertz frequencies. By applying the multiregion problem to the mode matching technique (MMT), the total reflection and transmission characteristics of the periodic MIM waveguide can be resolved as functions of the thickness of the MIM waveguide, the gap width of the MIM waveguide, the thickness of the quartz plate, and frequency. To validate the results of the proposed MMT, the transmission results are compared with the results using a commercial electromagnetic simulation software (XFdtd). The similar results demonstrate that the proposed MMT is proper to compute the reflection and transmission characteristics of the periodic MIM waveguide on the real quartz plate and providing in-depth intuition for resonant transmissions using the modal approach.

Introduction

Resonant transmission phenomena through the metallic slit have been sufficiently investigated while considering the negative permittivity of the metal in the terahertz (THz) regime [1]. Deep subwavelength Au and Ag slit transmittances at wide THz frequencies are analyzed [2,3], and the resonant transmission phenomena through periodic slits for the cases of various real metals are thoroughly investigated [4]. The transmittance behaviors at lower THz frequencies are similar to those in the perfect electric conductor (PEC) case, while greater discrepancies are found for higher frequencies. These findings constitute useful reference data for the deep subwavelength slit transmittances on metallic plates and can be applied to research areas such as spectroscopy [5,6], heat-assisted magnetic recording [7], optical data storage [8], and near-field scanning microscopy [9–11]. To apply the subwavelength slit structure to these areas, the transmission characteristics through single or periodic metallic slit should be validated. However, transmittance through the slit using only a metallic plate can be unsuitable because the metallic plate is too thin, and the subwavelength slit is too narrow in optical frequencies. Therefore, the supporting fixture is required to stabilize the thin metallic structure, and it is better for the fixture to have a low loss characteristic. The quartz (SiO_2) plate can be a good candidate because the quartz has little loss, and the transmittances through only the metallic slit can be predicted from those of the metallic slit with the quartz plate. In previous researches [2,3], the transmittances through only a metallic slit are investigated, however, a more in-depth study of the transmittances through the periodic slits including the quartz plate holding the metallic slit is required for practical purposes.

The transmittance problems can be analyzed by brute-force techniques like as finite-difference time-domain (FDTD) and finite element techniques [12,13]. However, these methods can only provide the transmittance results, and this is not sufficient for physical insight. On the other hand, the mode matching technique (MMT) [2,3,4,14,15] can be a good alternative, which provides how the modes in the metal-insulator-metal (MIM) waveguide are applied upon the boundary or through the slit. The advantages of the MMT can be listed as follows: (1) The brute-force numerical techniques such as FDTD or finite element method can obtain the transmittance results directly, but the physical meanings are not easily understood from them. By the MMT, the propagation characteristics can be easily and deeply understood and the field patterns for each mode can be also described. Moreover, the guide wavelengths of the MIM waveguide make it easy to understand the resonant transmittance as a function of the thickness of the metallic plate [2]. (2) The brute-force numerical techniques require a lot of mesh grids, so that the corresponding numerical dispersion error increases gradually at higher frequencies. The MMT, on the other hand, has the advantage of not requiring any grid and not having to worry about dispersion errors. In addition, the MMT can drastically reduce the simulation time. (3) When dealing with electromagnetic analyses for the real metals, the FDTD method is often used. In this case, Debye, Drude, or Lorentz models are used to describe metallic properties in the

* Corresponding author at: 94, Wausan-ro, Mapo-gu, Seoul 04066, Republic of Korea.
E-mail address: jongeon.park@gmail.com (J.-E. Park).
[1] Present address: 94, Wausan-ro, Mapo-gu, Seoul 04066, Republic of Korea.

https://doi.org/10.1016/j.rinp.2019.102881
Received 6 October 2019; Received in revised form 3 December 2019; Accepted 10 December 2019
Available online 14 December 2019

wide THz range. However, the Debye, Drude, or Lorentz models for the FDTD method cannot cover the wide THz frequency band. The MMT could be an alternative numerical technique for this layered problem since simply at each frequency the permittivities of the real metal and the quartz plate need to be replaced in our formulation.

In this paper, reflection and transmission characteristics through periodic metallic slits at THz frequencies are obtained by MMT [16], when the metallic plate is supported by the quartz plate. The proposed geometry has a four-layer structure, which consists of free-space, MIM waveguide, quartz plate, and another free-space. Practical permittivities for the real metal at two THz frequencies are considered. The incident, reflected, and transmitted electromagnetic fields are formulated to be applied to the MMT, and the multiregion problem [17] is introduced to solve multi-layer geometry. Then, reflection and transmission results for periodic slits are obtained when the metal in the MIM waveguide is a PEC or a real metal. Finally, we validate the transmittances for the real metal case and compare them with the results calculated by the commercial electromagnetic simulation software.

Problem geometry and dispersion equation

Fig. 1 displays the geometry of the proposed MIM structure with the quartz plate to investigate electromagnetic power transmissions and reflections. The proposed MIM structure is divided into four regions, which consists of free-space, MIM waveguide, quartz plate, and another free-space. Regions 1 and 4 are free-space, and Region 2 is the periodic MIM waveguide that resides between Junctions 1 and 2. The quartz plate is placed below the MIM waveguide and expressed as Region 3. The period (p) of the MIM waveguide is $2(g + d)$, the thickness of the MIM waveguide is w_1, and the type of metal considered in this work is

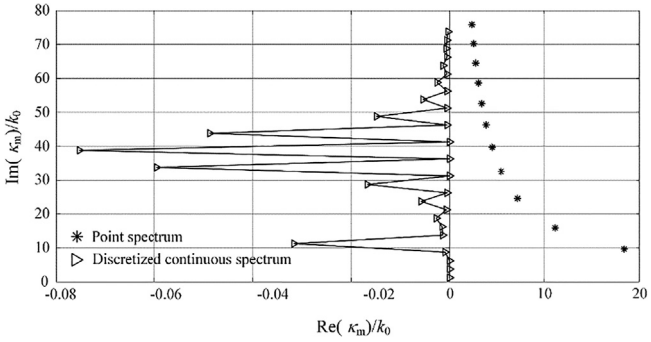

Fig. 2. Point (Asterisks) and discretized continuous (triangles) spectra in the geometry of Fig. 1.

silver (Ag) [18]. The quartz plate is located under the MIM waveguide with a thickness of w_2, which is inserted to support the metallic plate. The proposed structure is invariant along the y-axis and periodic with regard to the x-axis, and the incident wave is supposed to be a transverse magnetic (TM) wave along the z-axis. The transmission and reflection characteristics are observed according to the frequencies and thickness of the MIM waveguide plate. To compute the reflection and transmission characteristics about the proposed periodic MIM waveguide, the MMT is applied. The modes in the MIM waveguide are calculated and analyzed by the dispersion equation [2,14] as follows:

$$\tanh(\kappa_{i,n}g) = \frac{-\kappa_{m,n}/\varepsilon_m}{\kappa_{i,n}/\varepsilon_i}\tanh(\kappa_{m,n}d) \tag{1}$$

$$k_{z,n}^2 = \kappa_{m,n}^2 + \omega^2\mu\varepsilon_m = \kappa_{i,n}^2 + \omega^2\mu\varepsilon_i, \tag{2}$$

where ε_m and ε_i are permittivities in metal and insulator, respectively.

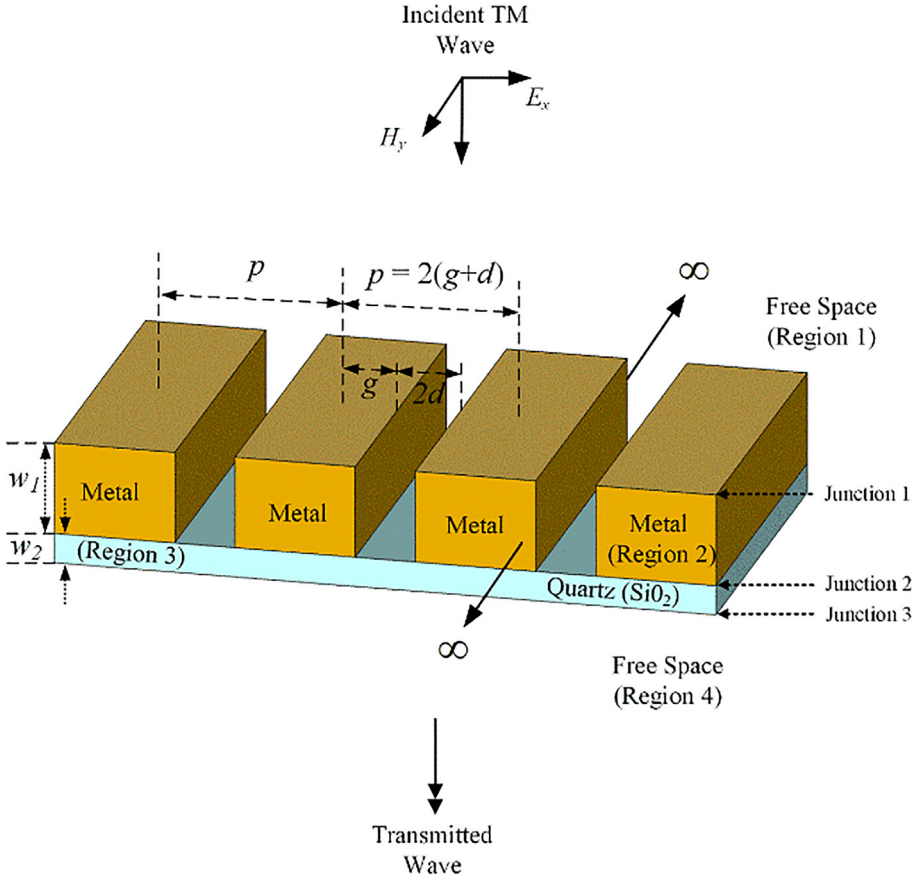

Fig. 1. Geometry of the proposed MIM structure with the quartz plate.

$k_{z,n}$ is the n-th propagation constant along the z-axis. $\kappa_{m,n}$ and $\kappa_{i,n}$ are the n-th transverse propagation constants in the metal and the insulator, respectively. The permittivities of the metal (Ag) are $-1470.8 - j355.65$ and $-94.108 - j7.567$ at 50 THz and 200 THz, respectively [18], and the insulator is fixed to free space ($\varepsilon_i = 1$). Fig. 2 represents the point spectrum (PS) (asterisk marker) and discretized continuous spectrum (DCS) (triangle marker) [2,14] in the proposed MIM structure when the period (p) is 0.6 λ_0, and 2 g is 0.2 λ_0 at 50 THz. Note that the real parts of each spectrum have a different positive and negative sign, and the scale is also different. When the real part of the PS has the largest value, it becomes the fundamental mode of the TM_0 in the MIM waveguide, which has the greatest impact on the transmission. In addition, a number of eigenvalues of the DCS will be applied in the MMT formulation. Although the DCS does not have a critical impact on the transmissions, it plays an important role by satisfying the boundary conditions. One more noteworthy point to mention from Fig. 2 is the relationship between the PS and the DCS. When the imaginary parts of the PS are between 30 and 50, the absolute values of real parts of the DCS become much greater. In other words, the distributions of PS recede the distributions of DCS, and this phenomenon is called the anti-crossing behavior [3,14]. It is a natural effort for PS and DCS modes to maintain orthogonal properties inherent in Eq. (1), even if it is not complete.

MMT and multiregion problem

To obtain the transmission characteristic of the proposed MIM structure, the solved modes in the periodic MIM waveguide are applied to the MMT, and the reflection and transmission coefficients can be computed for each Junction 1, 2, and 3. The electromagnetic fields at Junction 1, located between the free space and the MIM waveguide, can be arranged as:

$$a_k \vec{E}_{Fk} + \sum_{i=1}^{N_F} a_i \vec{E}_{Fi} = \sum_{j=1}^{N_M} b_j \vec{E}_{Mj} \tag{3a}$$

$$a_k \vec{H}_{Fk} - \sum_{i=1}^{N_F} a_i \vec{H}_{Fi} = \sum_{j=1}^{N_M} b_j \vec{H}_{Mj} \tag{3b}$$

where the $\vec{E}_{Fk}$ and $\vec{H}_{Fk}$ show the incident electric and magnetic fields of the k-th mode in Region 1, and the $\vec{E}_{Fi}$ and $\vec{H}_{Fi}$ represent the reflected electric and magnetic fields of the i-th mode in Region 1, respectively. The $\vec{E}_{Mj}$ and $\vec{H}_{Mj}$ also indicate the transmitted electric and magnetic fields of the j-th mode in Region 2. N_F and N_M are the overall number of those modes used in Regions 1 and 2. The subscripts F and M mean the free space and the MIM waveguide, respectively. An incident coefficient a_k, reflected coefficients a_i, and transmitted coefficients b_j are described in Eqs. (3a) and (3b). Here, a_k is a given coefficient, and the a_i and the b_j are the coefficients to be solved by Eqs. (3a) and (3b). The Eqs. (3a) and (3b) of the MMT can be applied only for a single frequency using the relative permittivity of the real metal at that THz frequency. The resonant transmission results at wide THz range can be obtained, if the relative permittivities of the real metal and quartz plate at each THz frequency are replaced in Eq. (1).

The reflection and transmission coefficients can be computed for each junction, however; it is important to obtain the total reflection and transmission coefficients considering all layers including the free space, the MIM waveguide, and the quartz plate. Fig. 3 shows the conceptual diagram of multiregion geometry to calculate the total reflection and transmission coefficients in Fig. 1. $R_{1,2}$ means the reflection coefficients in Region 1 reflected by Region 2 and $T_{1,2}$ stands for the transmission coefficients into Region 2 incident from Region 1. Similarly, $R_{2,1}$ and $T_{2,1}$ can be defined in reverse. All coefficients are represented by matrices because each region is composed of a lot of modes, and the generalized reflection coefficient in the proposed multiregion geometry

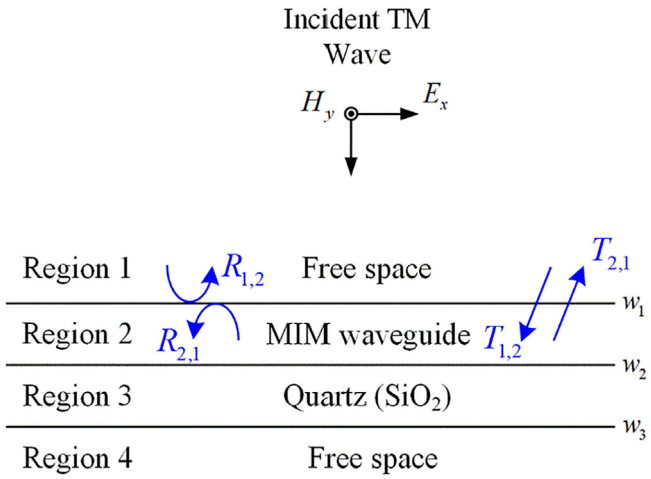

Fig. 3. Conceptual diagram of multiregion geometry.

can be expressed as [17]:

$$\tilde{R}_{m,(m+1)} = R_{m,(m+1)} + T_{(m+1),m} \cdot e^{-jK_{(m+1),z}(d_m - d_{m+1})} \cdot \tilde{R}_{(m+1),(m+2)} \cdot e^{-jK_{(m+1),z}(d_m - d_{m+1})} \cdot D_{(m+1)} \cdot T_{m,(m+1)} \tag{4}$$

$$D_{(m+1)} = \left[I - R_{(m+1),m} \cdot e^{-jK_{(m+1),z}(d_m - d_{m+1})} \cdot \tilde{R}_{(m+1),(m+2)} \cdot e^{-jK_{(m+1),z}(d_m - d_{m+1})} \right]^{-1}, \tag{5}$$

where the $K_{(m+1),z}$ and $D_{(m+1)}$ present the z-directional propagation constant and the multiple reflection effects along the z-axis in the $(m + 1)$ region, respectively, and the I stands for the identity matrix in the $(m + 1)$ region. In Eq. (4), the tilde refers to the generalized coefficient for considering the effects of the multiregion geometry while the $R_{m,(m+1)}$ without tilde stands for the reflection coefficient just at the junction between regions m and $(m + 1)$ without considering multiple reflections. Eqs. (4) and (5) can be utilized to compute the overall reflection and transmission powers for the proposed structure, which consists of the free space, the MIM waveguide, the quartz plate, and another free space.

Transmission and reflection characteristics

Fig. 4(a) presents the transmission and reflection power characteristics of the proposed periodic MIM waveguide structure in Fig. 1 when the metal is PEC. The peak transmittance is 0.9928 and the reflection power is 0.0072, when the thickness (w_2) of the quartz plate is 0.3λ_0. The peaks are repeatedly obtained with an interval of a half wavelength $(0.324 + 0.5n)\lambda_0$, where n is the integer, which is called as Fabry-Pérot resonance (FPR). The peaks are very close to 1 because the transmission resonance conditions are almost satisfied when the thicknesses of the MIM and the quartz plate are $(0.324 + 0.5n)\lambda_0$ and 0.3λ_0, respectively. The sum of the transmission and reflection powers is always 1, because the incident power is entirely contributed to both transmission and reflection powers and there is no loss in the PEC plate of the MIM waveguide. The peak transmissions decrease to 0.8647 when the thickness of the quartz plate becomes 0.9λ_0 as shown in Fig. 4(b), and the FPR is still observed with the interval of a half wavelength $(0.29 + 0.5n)\lambda_0$. The peak transmission power in Fig. 4(b) ($w_2 = 0.9\lambda_0$) is 0.1335 lower than that in Fig. 4(a) ($w_2 = 0.3\lambda_0$) because the transmission resonance condition is less satisfied when the thickness of the quartz is 0.9λ_0. The transmission characteristics of the periodic MIM waveguide, when the metal is PEC, are varied from 0.9982 to 0.8647 according to the thickness of the quartz, and the total power is always 1, which demonstrates that the proposed geometry satisfies the power

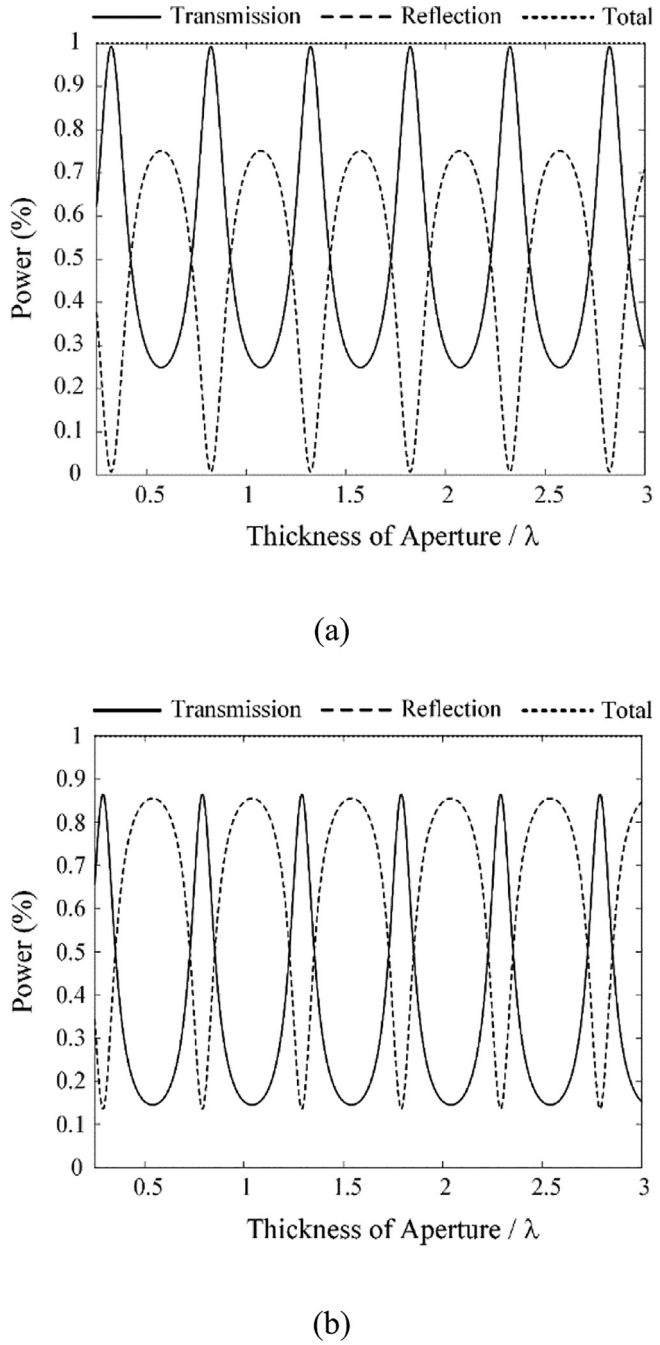

Fig. 4. Power of the proposed MIM structure when metal is PEC (a) $w_2 = 0.3\lambda_0$ (b) $w_2 = 0.9\lambda_0$.

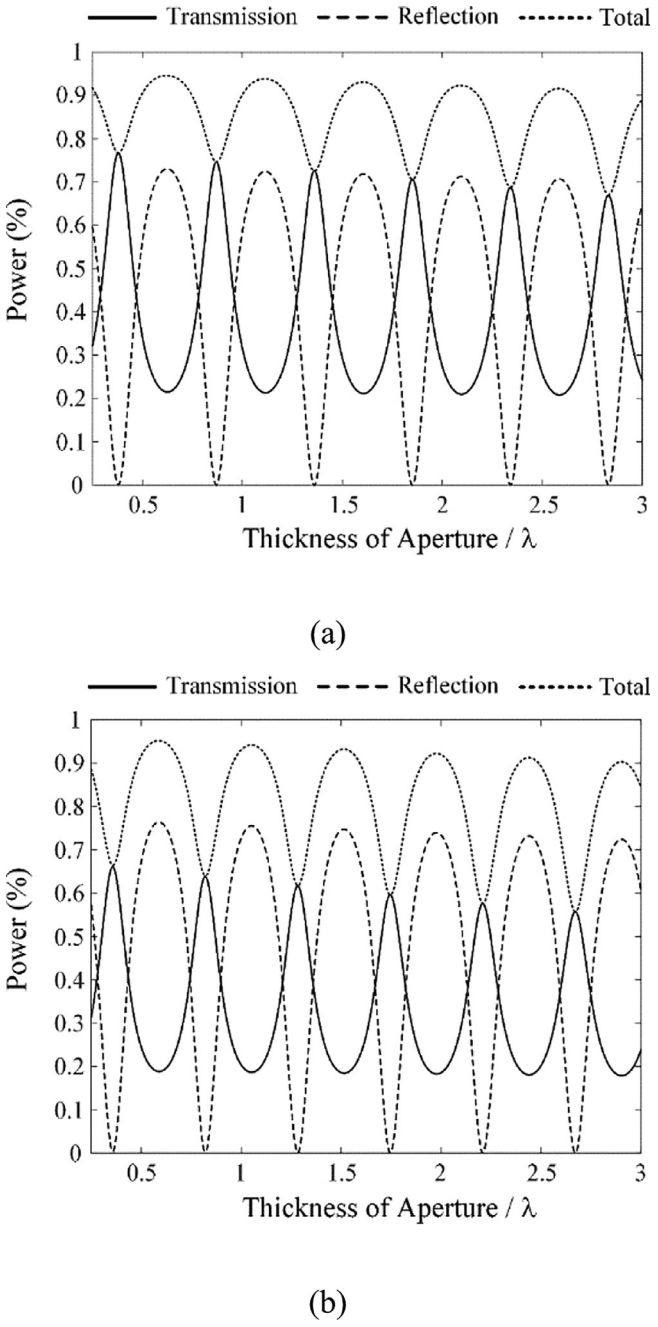

Fig. 5. Power of the proposed MIM structure when metal is silver (a) 50 THz (b) 200 THz.

conservation and does not suffer metallic loss.

Fig. 5(a) and (b) indicate the power transmission and reflection characteristics at 50 THz and 200 THz versus the thickness of the MIM plate, respectively, when the metal in the MIM plate is silver and the thickness of the quartz is $0.658\lambda_0$. The FPR phenomenon is also observed; however, the transmission maxima gradually decrease when the thickness (w_1) of the MIM waveguide increases from $0.25\lambda_0$ to $3\lambda_0$, because loss due to the silver plate arises when the electromagnetic wave passes the MIM waveguide. Power reflection characteristics are also observed in the dashed line, and the maxima of reflections arise whenever the minima of the transmissions are observed. The summation of the reflection and transmission is obtained by dotted lines, while the difference between the incident power (=1) and the dotted line becomes a loss from the silver plate in the MIM waveguide. As seen in Fig. 5, more electromagnetic waves pass through the MIM waveguide when the transmission maxima are observed, and more loss from the silver plate can be observed. The overall power transmissions at 200 THz are lower than those of 50 THz, because the loss by the silver plate at 200 THz is larger than the loss at 50 THz [18]. In other words, the transmittance characteristic at a lower frequency (50 THz) is closer to that in the PEC case, and greater discrepancies are observed for the higher frequency (200 THz).

Fig. 6 presents a comparison of the transmission characteristics between the MMT and the simulation results calculated by three-dimensional commercial electromagnetic software (XFdtd) from REMCOM [19]. To validate transmittances, the geometry in Fig. 1 is again applied when p is $0.6\lambda_0$ and 2 g is $0.2\lambda_0$. The thickness of the quartz plate is $0.658\lambda_0$, and a silver permittivity at 50 THz in the MIM waveguide is utilized. The maximum transmittance of the proposed

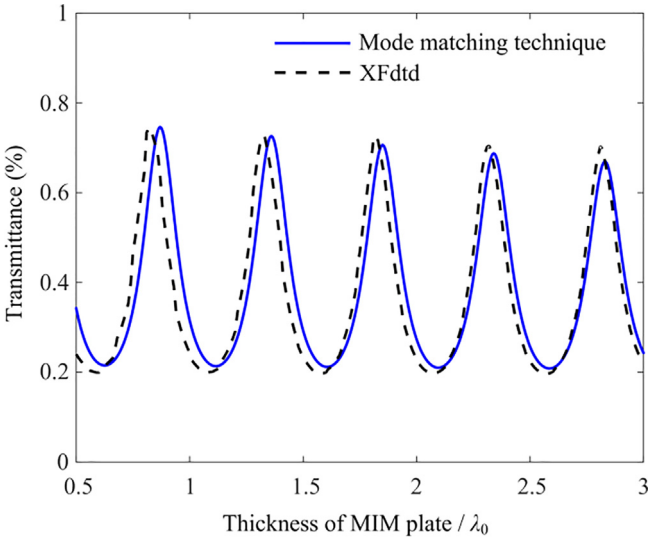

Fig. 6. Validation of transmittances (50 THz).

computation is 0.746, which is quite similar to the XFdtd value of 0.744, and the entire transmittance trends are also similar. Slight discrepancy in transmittances is discovered between the XFdtd and the MMT owing to the different numerical techniques. In spite of the delicate difference, the overall trends are fairly similar to each other, which demonstrates that the proposed MMT formulation is effective for analyzing the periodic metallic slits at THz frequencies as well as the multiregion geometry.

The MMT can be also applicable to the two-dimensional slit geometry, when the dimension in *y*-axis of Fig. 1 is limited to a single slit or arranged periodically.

Conclusion

We have investigated the resonant transmission through periodic subwavelength terahertz metallic slits based on the quartz plate. The transmission characteristics of the periodic MIM waveguide at 50 and 200 THz frequencies were investigated by the MMT. The proposed geometry was four-layered, consisting of free-space, MIM waveguide, quartz plate, and another free-space. Therefore, the multiregion problem was adopted to solve multi-layer geometry. When the metal became PEC, the peak transmittance of almost 1 was repeatedly observed at half wavelength intervals $(0.324 + 0.5n)\lambda_0$. On the other hand, lower peak transmittances of 0.766 and 0.661 are obtained at 50 THz and 200 THz, respectively, when the metal is silver. Moreover, the resonant transmission maxima gradually decreased as the thickness of the MIM plate increased from $0.25\lambda_0$ to $3\lambda_0$, due to the loss of the silver plate in the MIM waveguide.

CRediT authorship contribution statement

Sungjun Yoo: Data curation, Methodology, Software, Visualization, Writing - original draft. **Jong-Eon Park:** Conceptualization, Formal analysis, Methodology, Resources, Software, Supervision, Validation, Writing - review & editing. **Hosung Choo:** Funding acquisition, Investigation, Project administration, Writing - review & editing.

Declaration of Competing Interest

The authors declare that they have no known competing financial interests or personal relationships that could have appeared to influence the work reported in this paper.

Acknowledgements

This research was funded in part by the Nuclear Safety Research Program through the Korea Foundation Of Nuclear Safety (KoFONS) using the financial resource granted by the Nuclear Safety and Security Commission (NSSC) of the Republic of Korea (No. 1805006) and in part by the National Research Foundation of Korea (NRF) funded by the Ministry of Education (Nos. 2013R1A6A3A03022194, 2015R1A6A1A03031833, and 2017R1D1A1B04031890).

Appendix A. Supplementary data

Supplementary data to this article can be found online at https://doi.org/10.1016/j.rinp.2019.102881.

References

[1] Webb KJ, Li J. Analysis of transmission through small apertures in conducting films. Phys Rev B 2006;73(3):033401.
[2] Park J-E, Teixeira FL, Borges B-HV. Analysis of deep-subwavelength Au and Ag slit transmittances at terahertz frequencies. J Opt Soc Am B 2016;33(7):1355–64.
[3] Hur J, Choo H, Park J-E. Modal analysis of point and discretized continuous spectra for metal-insulator-metal waveguides in the terahertz region. J Electr Eng Technol 2018;13(4):1644–54.
[4] Yoo S, Park J-E, Choo H. Resonant transmission through periodic subwavelength real metal slits in the terahertz range. IEICE Electron Express 2018;15(14):20180612.
[5] Kuttge M, Cai W, de Abajo FJG, Polman A. Dispersion of metal-insulator-metal plasmon polaritons probed by cathodoluminescence imaging spectroscopy. Phys Rev B 2009;80(3):033409.
[6] Heer R, Rakoczy G, Ploner G, Strasser G, Gornik E, Smoliner J. Metal-insulator-metal injector for ballistic electron emission spectroscopy. Appl Phys Lett 1999;75(25):4007–9.
[7] Kryder MH, Gage EC, McDaniel TW, Challener WA, Rottmayer RE, Ju G, et al. Heat assisted magnetic recording. Proc IEEE 2008;96(11):1810–35.
[8] Chen F, Itagi A, Bain JA, Stancil DD, Schlesinger TE, Stebounova L, et al. Imaging of optical field confinement in ridge waveguide fabricated on very-small-aperture laser. Appl Phys Lett 2003;83(16):3245–7.
[9] Lin C-I, Gaylord TK. Multimode metal-insulator-metal waveguides: analysis and experimental characterization. Phys Rev B 2012;85(8):085405.
[10] Zhan H, Astley V, Hvasta M, Deibel JA, Mittleman DM, Lim Y-S. The metal-insulator transition in VO_2 studied using terahertz apertureless near-field microscopy. Appl Phys Lett 2007;91(16):162110.
[11] Verhagen E, Dionne JA, Kuipers L, Atwater HA, Polman A. Near-field visualization of strongly confined surface plasmon polaritons in metal-insulator-metal waveguides. Nano Lett 2008;8(9):2925–9.
[12] Ha S-G, Cho J, Lee J, Min B-W, Choi J, Jung K-Y. Numerical study of estimating the arrival time of UHF signals for partial discharge localization in a power transformer. J Electromagn Eng Sci 2018;18(2):94–100.
[13] Kim Y, Kim S, Kim D-S, Oh I-Y, Yook J-G. Numerical investigation of scattering from a surface dielectric barrier discharge actuator under atmospheric pressure. J Electromagn Eng Sci 2018;18(1):52–7.
[14] Kocabas SE, Veronis G, Miller DAB, Fan S. Modal analysis and coupling in metal-insulator-metal waveguides. Phys Rev B 2009;79(3):035120.
[15] Sturman B, Podivilov E, Gorkunov M. Eigenmodes for metal-dielectric light-transmitting nanostructures. Phys Rev B 2007;76(12):125104.
[16] Wexler A. Solution of waveguide discontinuities by modal analysis. IEEE Trans Microw Theory Tech 1967;15(9):508–17.
[17] Chew WC. Waves and fields in inhomogeneous media. Wiley; 1999.
[18] Rakic AD, Djurisic AB, Elazar JM. Majewski ML Optical properties of metallic films for vertical-cavity optoelectronic devices. Appl Opt 1998;37(22):5271–83.
[19] Remcom: XFdtd 3D electromagnetic simulation software; 2019. http://www.remcom.com.